Geophysical Research Letters

RESEARCH LETTER
10.1029/2022GL098792

Turbulence Effects on the Formation of Cold Fog Over Complex Terrain With Large-Eddy Simulation

Xin Li[1] and Zhaoxia Pu[1]

[1]Department of Atmospheric Sciences, University of Utah, Salt Lake City, UT, USA

Key Points:

- Large-scale turbulent eddies are critical for fog formation over complex terrain
- Turbulent eddies exist under stable planetary boundary layer|planet boundary layer (PBL) and can help mixing effects, thus enhancing conditions for fog formation over complex terrain
- Omission of turbulent eddies in the PBL parameterization scheme results in weak mixing effects in the PBL, thus failing to simulate the fog

Supporting Information:

Supporting Information may be found in the online version of this article.

Correspondence to:

Z. Pu,
Zhaoxia.Pu@utah.edu

Citation:

Li, X., & Pu, Z. (2022). Turbulence effects on the formation of cold fog over complex terrain with large-eddy simulation. *Geophysical Research Letters*, *49*, e2022GL098792. https://doi.org/10.1029/2022GL098792

Received 20 MAR 2022
Accepted 17 MAY 2022

Author Contributions:

Conceptualization: Zhaoxia Pu
Data curation: Xin Li, Zhaoxia Pu
Formal analysis: Xin Li, Zhaoxia Pu
Funding acquisition: Zhaoxia Pu
Investigation: Xin Li, Zhaoxia Pu
Methodology: Xin Li, Zhaoxia Pu
Project Administration: Zhaoxia Pu
Resources: Zhaoxia Pu
Software: Xin Li
Supervision: Zhaoxia Pu
Validation: Xin Li, Zhaoxia Pu
Visualization: Xin Li

Abstract A large eddy simulation (LES) embedded in the mesoscale community Weather Research and Forecasting model is used to examine the effects of turbulence on cold fog formation over Heber Valley in northern Utah in the U.S. The LES results indicate that large-scale turbulent eddies prevail and dominate the mixing effects in the planetary boundary layer (PBL). The combination of turbulence mixing effects, mountain-valley flow, and ultra-cold valley temperature lead to fog formation in the LES simulation. The omission of the turbulent eddies in the PBL parameterization results in a weak mixing effect in the PBL and weakens the near-surface air cooling, thus failing to reproduce the fog in the simulation. This study indicates the essential role of turbulence in fog formation over complex terrain. Turbulent eddies exist over complex terrain and can enhance mixing effects, and thus the conditions for fog formation.

Plain Language Summary Turbulence mixing can affect the temperature and moisture exchange in the atmospheric boundary layer, the lower part of the atmosphere near the earth's surface. The planetary boundary layer parameterization scheme of mesoscale models cannot resolve the contributions of turbulent eddies to weather phenomena due to the coarser grid spacing of mesoscale models. This study conducted a large-eddy simulation at fine resolution to simulate a fog event over the Heber Valley. It is found that large-scale turbulent eddies are critical for fog formation over complex terrain.

1. Introduction

Fog is a meteorological hazard that can significantly reduce visibility near the surface to less than 1 km (American Meteorological Society, 2012). Low visibility caused by condensed water droplets and/or ice crystals severely impacts traffic and human life, causing substantial economic losses comparable to storms and tornados (Gultepe et al., 2007). However, fog is associated with multiple physical and dynamic processes, such as microphysics (MP), the land surface, the planet boundary layer (PBL), radiation, and their interaction, making accurate fog prediction a challenge (Bergot & Guedalia, 1994; Guedalia & Bergot, 1994; Lin et al., 2017; Román-Cascón et al., 2016, 2019; Steeneveld et al., 2015; Tudor, 2010; Van der Velde et al., 2010; Zhou et al., 2012), especially over complex terrain (Gultepe et al., 2007, 2009, 2015, 2016; Müller et al., 2010; Price, 2011; Pu, 2017; Pu et al., 2016).

During the winter, the ultra-cold land surface makes the surface air especially cold and results in the formation of ephemeral fog near the valley surface. Numerical weather prediction models have difficulty capturing this type of fog in simulations. For instance, during a recent field project, the Mountain Terrain Atmospheric Modeling and Observations (MATERHORN) Program in January–February 2015 (Fernando et al., 2015; Gultepe et al., 2016), fog in the region was well simulated by the mesoscale community Weather Research and Forecasting (WRF) model (Skamarock et al., 2019), but poorly reproduced over the Heber Valley in northern Utah in the United States due to the inadequate representation of near-surface atmospheric conditions and boundary layer structure (Pu et al., 2016). In a follow-on study, Zhang and Pu (2019) found that increased snow cover and snow depth in the model could increase the albedo and slightly reduce the near-surface temperature, which led to favorable conditions for fog formation. However, fog was still absent in the simulation, indicating that the cloud-permitting-scale mesoscale model (~1 km horizontal resolution) is inadequate for fog prediction. With the parameterized PBL scheme, smaller-scale processes (such as turbulence mixing) are missed in mesoscale simulations.

Previous studies have found that fog simulation is not significantly different in simulations with different PBL schemes (Chachere & Pu, 2018; Chaouch et al., 2017; Chen et al., 2020; Pithani et al., 2019; Román-Cascón et al., 2012). The PBL scheme, whether non-local or local, cannot simulate turbulent eddies directly but only parameterizes their averaged subscale contributions. Therefore, the omission of fog over the Heber Valley in the

Writing – original draft: Xin Li
Writing – review & editing: Zhaoxia Pu

numerical simulation could be related to the inadequacy of the WRF simulation with the PBL scheme in simulating turbulent eddies. From the MATERHORN-fog observations, Hang et al. (2016) found a prevailing gravity wave (GW) in the Heber Valley. Uematsu et al. (2005) indicated that a GW can associate with turbulence to form fog. Therefore, it is necessary to investigate the role of turbulent mixing (TB) in fog formation.

The recent development of large eddy simulation (LES) offers a great opportunity to study the impact of turbulence on fog formation. Fog simulations performed by LES (Bergot, 2016; Maronga & Bosveld, 2017; Mazoyer et al., 2017; Porson et al., 2011) indicate that LES usually generates a better PBL structure and makes better fog predictions (Cui et al., 2019; Mazoyer et al., 2017), compared to simulations with PBL schemes. The association of turbulence with the fog layer (Bergot, 2013; Nakanishi, 2000) has also been identified. However, *the effect of turbulence in fog formation*, *especially over complex terrain*, *has not yet been emphasized*. In this study, we use the WRF embedded LES (WRF-LES) to simulate a fog event over the Heber Valley on 16 January 2015 and compare it with the WRF simulation. In particular, we examine for the first time the turbulence mixing effect on the formation of cold fog in the Heber Valley, Utah, a valley in complex mountainous terrain.

2. WRF-LES Simulation and Analysis Method

The one-way nested WRF-LES model (version 4.3) is used to simulate the cold fog over the Heber Valley on 16 January 2015. In the simulation, five-level nested domains were configured with grid meshes (horizontal resolution) of 201 × 152 (25 km), 301 × 301 (5 km), 601 × 601 (1 km), 501 × 501 (200 m), and 201 × 201 (40 m), respectively. The outer three domains were set up with the Yonsei University (YSU) PBL parameterization scheme (Hong, 2010; Hong et al., 2006), and no PBL scheme was used in the inner two domains, but the three-dimensional turbulence kinetic energy 1.5 closure scheme was used to derive sub-scale turbulence. The Kain and Fritsch (Kain, 2004) deep convection scheme was activated only in domain one. Other physical schemes were used including the Thompson cloud microphysical scheme (Thompson et al., 2004), the Rapid Radiative Transfer Model (RRTM, Mlawer et al., 1997) for long-wave radiation, the Dudhia scheme (Dudhia, 1989) for short-wave radiation, the Noah land-surface scheme (Chen and Dudhia, 2001), and the revised MM5 Monin-Obukhov scheme for surface parameterizations.

The National Centers for Environmental Prediction (NCEP) North American Mesoscale Forecast System (NAM) 12 × 12 km analysis product is used to derive the initial and boundary conditions. Sixty-eight vertical levels, in which 33 levels are below 1,500 m, are used in the first four domains, and 74 vertical levels, with the lowest model level at approximately 2 m, are used in domain 5. Based on observations, fog occurred from 0735 to 1435 UTC on 16 January 2015. The initial time of the model is set at 00 UTC 15 January 2015 for a 24 hr spin-up.

For the first three domains, the turbulence contribution was generated from the YSU scheme. For the LES domains, a horizontal averaging method (5 × 5 grid average for domain 4 and 25 × 25 grid average for domain 5) was introduced into the simulation results to generate mean fields (Li et al., 2021). The variables—u, v, w, t, q, etc.—were averaged with this method, and the turbulence field with turbulent eddy signals was then produced by subtracting the mean field from the original field.

3. Simulation Result

Observations indicate that fog occurred over the Heber Valley (111°24'W, 40°30'N) from 0735 to 1435 UTC 16 January 2015. First, the simulation result from WRF with YSU PBL scheme (WRF, hereafter) and LES simulation using WRF-LES (LES, hereafter) are compared to the observations. Results show that WRF missed the fog in the simulation, while LES successfully simulated fog formation at 0730 UTC 16 January 2015 and its evolution afterward. To validate the simulation, the simulated liquid water content (LWC) from domains 1–4 is compared to the NOAA High-Resolution Rapid Refresh (HRRR, at 3 km horizontal resolution) analysis product at 0900 UTC 16 January 2015 at a height of 50 m, the level at which HRRR resolved the distribution of fog (Figure 1). The Heber Valley is approximately in the center of Figures 1a–1e. The HRRR analysis is the finest-resolution operational regional analysis available and provides reliable analysis (e.g., Bytheway et al., 2017). At 0900 UTC, HRRR analysis indicates that fog is spread around the Heber Valley with an LWC of about 0.06 g kg^{-1} due to the saturation (Figure 1a). With low values (nearly 0) of LWC, it is clear that no fog is reproduced in domains 1–3 over the Heber Valley (Figures 1b–1d). This result is consistent with the WRF simulation in Pu et al. (2016) and

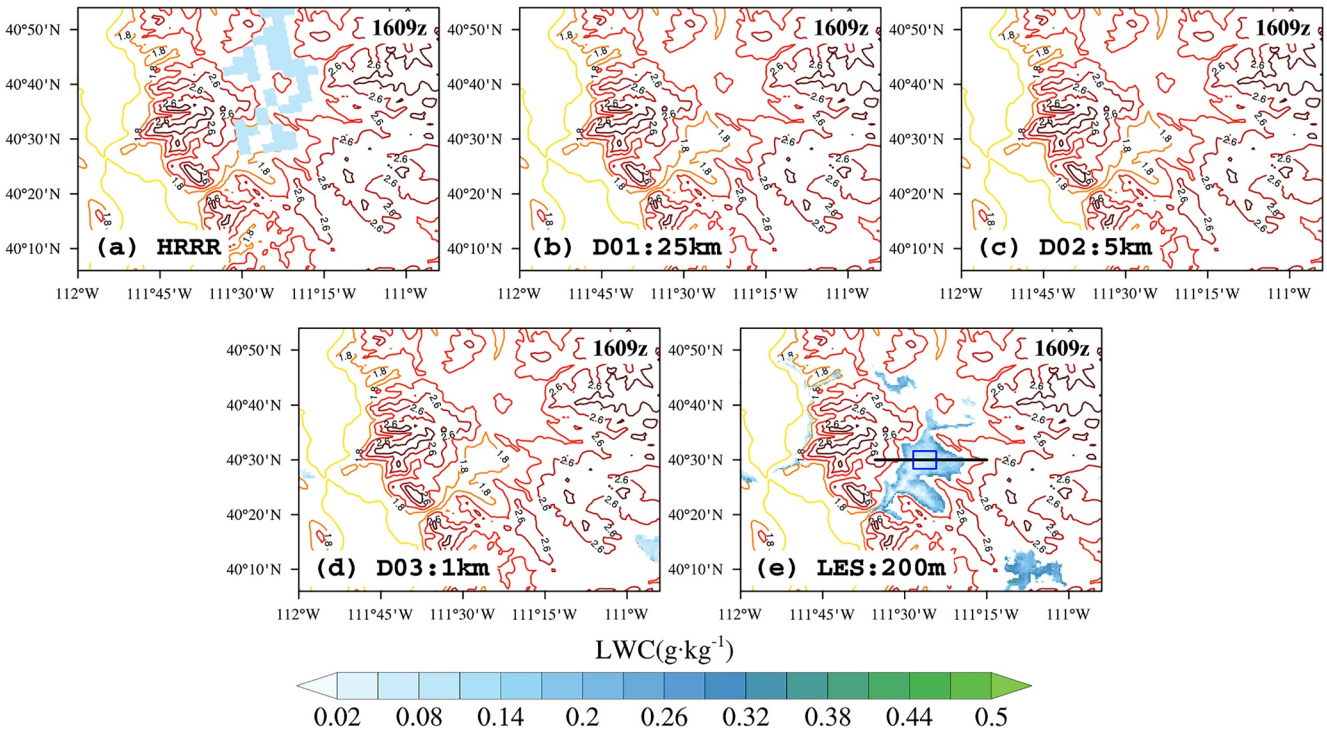

Figure 1. Liquid water content (LWC, shaded contour) at 50 m height from (a) High-Resolution Rapid Refresh (HRRR) analysis and simulations of (b) domain 1, (c) domain 2, (d) domain 3, and (e) domain 4 at 0900 UTC on 16 January 2015. The terrain height is added as line contour (unit: km). The blue box in (e) stands for the region of domain 5, which has the similar LWC values as in domain 4 (not shown). The black line in (e) represents the cross-section in Figures 4a–4c.

Zhang and Pu (2019). Large eddy simulation, namely, the simulations in domains 4 and 5, generates fog in the Heber Valley with a similar LWC (Figure 1e) compared to HRRR (Figure 1a).

To further evaluate the difference between the WRF and LES simulations, the simulated profiles of wind, air temperature, and relativity humiditylrelative humidity (RH) are compared to the sounding data over the Heber Valley (Figure 2) at 1115 UTC 16 January 2015. Specifically, during the fog events, the wind is mostly less than 2 m s^{-1}. The simulation from domains 3–5, especially the LES of domains 4–5, generates a low wind similar to the observations, whereas simulations from domains 1–2 reproduce a wind profile slightly different from the observations (Figure 2a). The air temperature sounding indicates an inversion layer with very cold air below 350 m, which drops to −12°C below 100 m. The near-surface air temperature profiles from domains 1–3 do not show this inversion layer, and the temperature goes down to only around 0°C, far above the observed temperature of −10 to −11°C. However, the LES in domains 4 and 5 generates near-surface air temperature profiles that are much closer to the observations, with the cold air of −6°C (Figure 2b) near the surface. With the cold air temperature and associated high RH (nearly 100%), which are much closer to observations than those generated by WRF, LES has successfully simulated the fog event. According to Gultepe et al. (2015), cold fog can form under temperatures below −10°C when RH exceeds 80%. In the study case, the observed near-surface temperature below −10°C and RH reached nearly 90% met the cold fog criterion. Meanwhile, although slightly different from the observations, with near-surface temperature about −6°C and 100% RH, the LES simulation also indicated the fog formation.

In contrast, the warm temperature and low RH from the WRF (domain 1–3) prevent fog formation over the Heber Valley. In Pu et al. (2016) and Zhang and Pu (2019), the WRF simulation also generates similar warm air over the Heber Valley. Although Zhang and Pu (2019) increased the snow depth and albedo to slightly decrease the near-surface air temperature, the fog was still absent over the Heber Valley. The LES in this study further reduces the near-surface air temperature and finally leads to fog formation.

Figure 3 shows the 2 m wind, air temperature, and RH and surface wind time series from WRF and LES over the Heber Valley against surface Mesonet observations. The surface Mesonet observation indicates cold, high-RH air

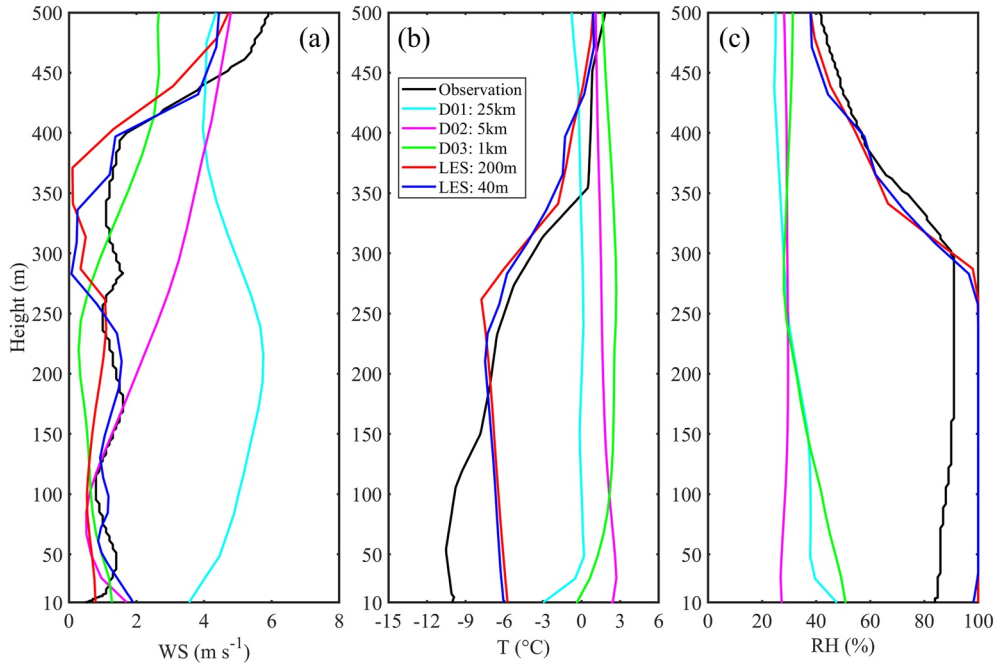

Figure 2. Vertical profiles of (a) wind speed, (b) air temperature, and (c) relative humidity (RH) from simulations against the sounding data over the Heber Valley at 1115 UTC on 16 January 2015.

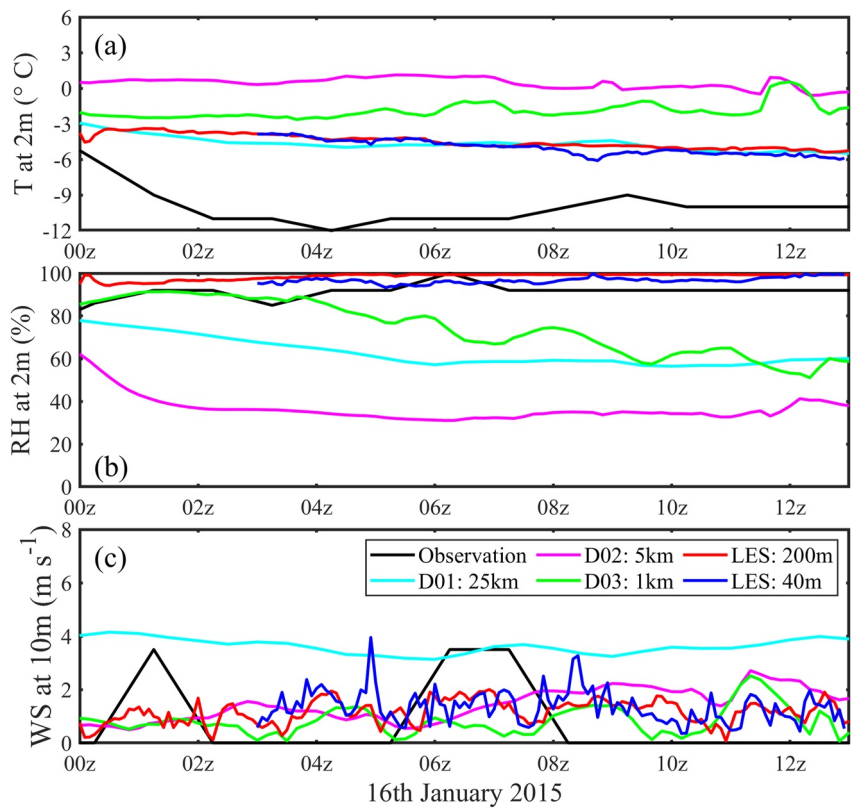

Figure 3. Time series of 2 m (a) air temperature, (b) relative humidity (RH), and (c) 10 m wind speed from simulations against the observations over the Heber Valley on 16 January 2015.

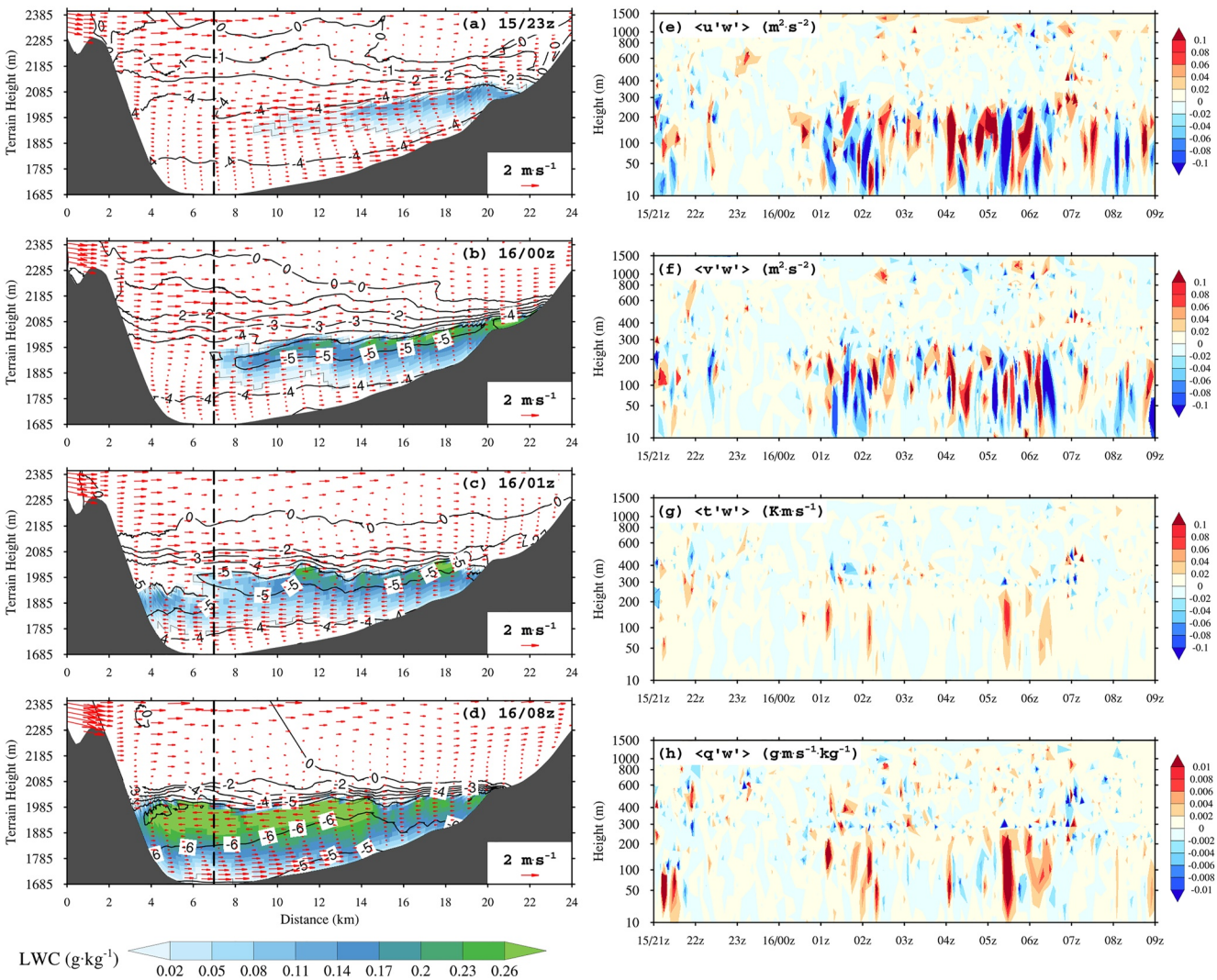

Figure 4. (a–d) East-west cross-section (through the black line in Figure 1e) of the simulated liquid water content (LWC) (shaded color contours), horizontal flow (vectors), and temperature (contour interval 1°C) before the fog formation at (a) 2300 UTC on 15 January, (b) 0000 UTC on 16 January, and (c) 0100 UTC on 16 January 2015, and during the fog formation at (d) 0800 UTC on 16 January 2015. Mountainous terrain is shaded black. (e–h) Evolution of the simulated flux of the (e) momentum flux component <u'w'>, (f) momentum flux component <v'w'>, (g) <t'w'>, and (h) <q'w'> based on domain 5 at the site station marked by the black dashed line in a–d from 21 UTC 15 January to 09 UTC 16 January 2015.

over the Heber Valley with low wind. Compared to the WRF in domain 1–3, the LES in domain 4 and 5 generates air temperature and RH closer to the observations. The cold, moist air favors fog formation; thus, LES reproduced fog in the simulations.

4. Turbulence Effects

To clarify the mechanism of fog formation in LES, Figures 4a–4d shows a cross-section (along the black line in Figure 1e) of LWC, horizontal flow vectors, and temperature in the Heber Valley at 2300 UTC 15 January and 0000, 0100, and 0800 UTC 16 January 2015 from LES. From Figures 4a–4d, it is apparent that the fog forms on the east side of the mountain and is transported aloft to the valley area by horizontal winds, and then it is gradually transported down to the ground. After sunset at around 2,300 UTC 15 January, mountain surface cooling creates saturated water vapor near the east side of the mountain at a terrain height of ~2,000 m (Figure 4a). This saturated water vapor (supercooled water) gradually spreads in the valley aloft following the easterly winds at the same level. Below that height, near-surface winds blow upslope (westerly) and prevent the saturated water vapor

from being transported over the valley floor. At 0000 UTC 16 January, the saturated water vapor spreads over most of the valley aloft. The mountain surface winds still blow upslope, and the winds are calm in the valley. At the height of ~2,000 m, the easterly winds near the east side of the mountain become weaker, and the westerly winds near the west side of the mountain become stronger. At 0100 UTC 16 January, the saturated water vapor spreads over the whole valley aloft. The near-surface winds become very weak all around. At the height of ~2,000 m, the westerly winds dominate. From 2300 UTC 15 January to 0100 UTC 16 January, there is a neutral-stable layer between the height of 1,780 m (~100 m above the valley floor) and 2,050 m, enveloped by the −4°C contour line, which traps all the saturated water vapor (fog) inside so it does not spread to the ground. The surface winds are still calm. Then, after 0100 UTC 16 January, corresponding to the radiative cooling at the fog top during the evening and night, the near-surface air temperature decreases. Downslope winds are established near the mountain surface. At 0800 UTC 16 January, the wind speed is about 1 m s^{-1} near the valley floor, and the near-surface temperature drops to below −6°C. The ultra-cold near-surface temperature enhances the saturated water vapor. The saturated water vapor spreads well over the valley floor, indicating fog formation in the Heber Valley. In contrast, the WRF simulation does not produce all the fine structure of the local flow pattern, cold temperatures, and saturated water vapor (see Figure S1 in Supporting Information 1); thus it fails to predict the fog formation.

During the whole period as described above, vertical winds are minimal throughout the mountain valley. Although mountain-valley flow and ultra-cold valley temperature both play roles in the fog formation, the mechanism that causes the downward extension of the saturated water vapor (fog) still needs to be clarified. Figures 4e–4h shows the evolution of the LES-simulated turbulent flux of momentum <u'w'> and <v'w'>, air temperature <t'w'>, and specific humidity <q'w'> at the valley sounding location (as in Figure 2) as indicated by the black dashed line in Figures 4a–4d. Below the height of 300 m, there is a strong momentum flux (magnitude over 0.1 m^2 s^{-2}) at the valley floor after 0000 UTC 16, when the mountain fog spreads the over the valley aloft. The extremely intense momentum flux at around 0100 UTC and 0600 UTC is associated with the large temperature (i.e., <t'w'>) and moisture (i.e., <q'w'>) fluxes, implying the influence of radiative cooling at the fog top on the near-surface temperature and the moisture flux between near the fog formation time (0500 and 0700 UTC). These fluxes from the LES simulation are much stronger than that from the WRF simulation, which is often near zero (not shown) during the whole period (not shown).

The stronger turbulence fluxes in the LES imply a stronger turbulence mixing effect that could mix the air well, including air temperature and humidity in the PBL, and help the fog spread downward. In the Heber Valley, there is often a GW when air flows over the surrounding mountains (Hang et al., 2016). This GW can regenerate some large-scale turbulence through wind shear at high levels. Under neutral-stable conditions, namely, the fog period, large-scale turbulent eddies (wavelength of over 100 m) are usually hard to decompose to small-scale turbulent eddies due to the weak wind shear near the surface, making large-scale turbulent eddies dominant in the vertical mixing effect (Li et al., 2020). The turbulent eddies here also have a large scale, with a wavelength of 40–300 m due to the weak wind near the surface (shown in Figures 2a and 3c, and 4a–4d). These large turbulent eddies (e.g., Figures 4e and 4f), including thermodynamic turbulent eddies (e.g., Figures 4g and 4h), mix the near-surface air well and decrease the air temperature to create saturation conditions there, resulting in fog formation. However, in the WRF simulation, conducted with the YSU PBL scheme, the parameterized turbulence is too weak in the PBL and weakens the vertical mixing of cold air, causing the fog over the Heber Valley to be missed.

To further examine the role of turbulence effects, Figure 5 shows the LWC tendency from advection (ADV), turbulence (TBL), and MP contributions at the same site as in Figures 4e–4h before (0100 UTC and 0530 UTC), near (0730 UTC), and after (0930 UTC) the fog formation. At 0100 UTC 16 January, saturated water vapor has already been spread in the valley aloft but does not reach the surface. The ADV contribution is small below 250 m height and slightly larger between 250 and 300 m with a negative impact. The contribution of both TBL and MP are larger than the ADV contribution. The turbulence transports the LWC from 200 to 300 m (negative LWC tendency) to 50–200 m (positive LWC tendency), while microphysical processes continue to saturate the water vapor (positive LWC tendency) at the height of 200–300 m. At 0530 UTC 16 January, the ADV contribution is minimal. There is also a strong tendency to transport the LWC from the layer at 250–350 m height to the layer at 150–200 m. The turbulence also transports the LWC downward, with positive LWC tendency below about 50 m height and negative LWC tendency above; this encourages fog formation near the surface. Meanwhile, above 50 m, the MP contribution is still significant and positive in most areas to supply the LWC, corresponding to the cooling of the air at that time. Then, at 0730 UTC, with the fog formed by that time, the ADV contribution

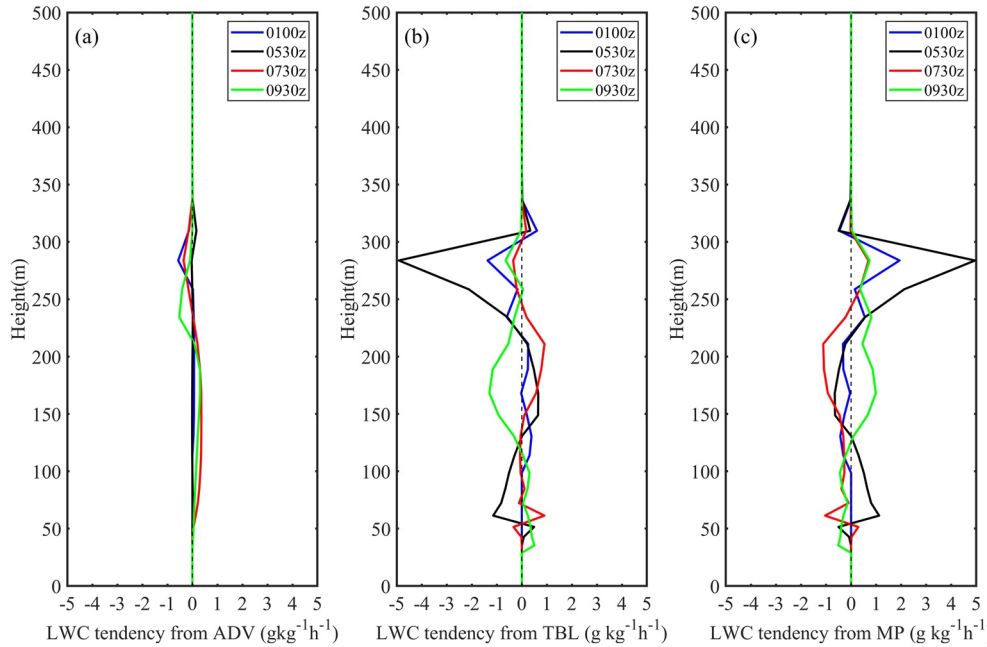

Figure 5. The liquid water content (LWC) tendency from the contribution of (a) advection (ADV), (b) turbulent mixing (TBL), and (c) microphysics (MP) over the Heber Valley at 0100, 0530, 0730, and 0930 UTC 16 January 2015 based on domain 5.

gradually turns positive at 50–200 m. The turbulence effects still positively contribute to LWC below 250 m. The MP contribution decreases by that time. At 0930 UTC, during the mature phase of the fog, both ADV and turbulence continue to positively contribute to the LWC near the surface to maintain the fog, although the microphysical contribution is slightly negative near the surface. The findings here confirm the significant impact of the turbulence mixing effect in the Heber Valley fog event. The missing of some turbulent eddies in the WRF PBL parameterization scheme leads to the failure of the fog simulation. The LES reproduces the turbulence and leads to fog formation in the simulation.

5. Summary and Conclusion

In this study, a one-way nested WRF-LES model was used to examine the influence of PBL turbulence on cold fog formation over the Heber Valley in northern Utah in the United States on 16 January 2015. During the fog event, the near-surface air temperature dropped to −12°C at night, favoring the formation of cold fog in the Heber Valley. Neither a previous WRF simulation (Pu et al., 2016; Zhang & Pu, 2019) nor the WRF simulation with PBL parameterization in this study captured the cold near-surface temperature, and thus both failed to reproduce the fog. However, the LES successfully simulated the fog event. Results indicate that large-scale turbulent eddies prevail and dominate the mixing effect in the PBL. The combination of turbulence mixing effects, mountain-valley flow, and ultra-cold valley temperature lead to the fog formation in the LES simulation. The omission of the turbulent eddies in the PBL parameterization scheme results in a weak mixing effect in the PBL and weakens the near-surface air cooling, resulting in the eventual failure to reproduce the fog in the numerical simulation.

While previous studies have found that turbulence in the PBL, such as horizontal rolls, can generate fog under near-saturated conditions similar to a roll-induced cloud street (Uematsu et al., 2005; Welch & Wielicki, 1986), this study further indicates that the existence of turbulent eddies can help mix the composition and favor fog formation under cold conditions. Numerical fog prediction over complex terrain should consider the impact of turbulence on fog formation. Future work should emphasize more fog cases over complex terrain and develop more realistic parameterization schemes.

Data Availability Statement

The National Centers for Environmental Prediction North American Mesoscale Forecast System data are obtained from the National Center for Atmospheric Research (NCAR) Research Data Archive (https://rda.ucar.edu/datasets/ds609.0/). The meteorological and surface Mesonet data (e.g., NOAA Earth System Research Laboratory (ESRL) Metetorologicsal Assimilation Data Ingest System (MADIS) Mesonet Data) can be obtained from the NCAR Earth Observing Laboratory (EOL) data archive (https://data.eol.ucar.edu/). The software of Weather Research and Forecasting (WRF)-large eddy simulation (version 4.3) can be obtained from WRF User's website (https://www2.mmm.ucar.edu/wrf/users). Information about High-Resolution Rapid Refresh analysis can be found from https://rapidrefresh.noaa.gov/hrrr/.

Acknowledgments
This study is supported by U.S. National Science Foundation Award # AGS-2049100, Cold Fog Amongst Complex Terrain (CFACT). The computational resources and support from the University Cooporation for Atmospheric Research (UCAR) Computational and Information Systems Lab (CISL) supercomputing system and the Center for High-Performance Computing at the University of Utah are appreciated.

References

American Meteorological Society. (2012). *Glossary of meteorology*. Retrieved from http://glossary.ametsoc.org

Bergot, T. (2013). Small-scale structure of radiation fog: A large-eddy simulation study. *Quarterly Journal of the Royal Meteorological Society*, *139*(673), 1099–1112. https://doi.org/10.1002/qj.2051

Bergot, T. (2016). Large-eddy simulation study of the dissipation of radiation fog. *Quarterly Journal of the Royal Meteorological Society*, *142*(695), 1029–1040. https://doi.org/10.1002/qj.2706

Bergot, T., & Guedalia, D. (1994). Numerical forecasting of radiation fog. Part I: Numerical model and sensitivity tests. *Monthly Weather Review*, *122*(6), 1218–1230. https://doi.org/10.1175/1520-0493(1994)122%3C1218:NFORFP%3E2.0.CO;2

Bytheway, J. L., Kummerow, C. D., & Alexander, C. (2017). A features-based assessment of the evolution of warm season precipitation forecasts from the HRRR model over three years of development. *Weather and Forecasting*, *32*(5), 1841–1856. https://doi.org/10.1175/WAF-D-17-0050.1

Chachere, C. N., & Pu, Z. (2018). Numerical simulations of an inversion fog event in the Salt Lake Valley during the MATERHORN-fog field campaign. *Pure and Applied Geophysics*, *176*(5), 2139–2164. https://doi.org/10.1007/s00024-018-1770-8

Chaouch, N., Temimi, M., Weston, M., & Ghedira, H. (2017). Sensitivity of the meteorological model WRF-ARW to planetary boundary layer schemes during fog conditions in a coastal arid region. *Atmospheric Research*, *187*, 106–127. https://doi.org/10.1016/j.atmosres.2016.12.009

Chen, C., Zhang, M., Perrie, W., Chang, R., Chen, X., Duplessis, P., & Wheeler, M. (2020). Boundary layer parameterizations to simulate fog over Atlantic Canada waters. *Earth and Space Science*, *7*(3), e2019EA000703. https://doi.org/10.1029/2019EA000703

Chen, F., & Dudhia, J. (2001). Coupling an advanced land surface–hydrology model with the Penn State–NCAR MM5 modeling system. Part I: Model implementation and sensitivity. *Monthly Weather Review*, *129*(4), 569–585. https://doi.org/10.1175/1520-0493(2001)129<0569:CAALSH>2.0.CO;2

Cui, C., Bao, Y., Yuan, C., Li, Z., & Zong, C. (2019). Comparison of the performances between the WRF and WRF-LES models in radiation fog–A case study. *Atmospheric Research*, *226*, 76–86. https://doi.org/10.1016/j.atmosres.2019.04.003

Dudhia, J. (1989). Numerical study of convection observed during the winter monsoon experiment using a mesoscale two-dimensional model. *Journal of the Atmospheric Sciences*, *46*(20), 3077–3107. https://doi.org/10.1175/1520-0469(1989)046<3077:NSOCOD>2.0.CO;2

Fernando, H. J. S., Pardyjak, E. R., Di Sabatino, S., Chow, F. K., De Wekker, S. F. J., Hoch, S. W., et al. (2015). The MATERHORN: Unraveling the intricacies of mountain weather. *Bulletin of the American Meteorological Society*, *96*(11), 1945–1967. https://doi.org/10.1175/BAMS-D-13-00131.1

Guedalia, D., & Bergot, T. (1994). Numerical forecasting of radiation fog. Part II: A comparison of model simulation with several observed fog events. *Monthly Weather Review*, *122*(6), 1231–1246. https://doi.org/10.1175/1520-0493(1994)122<1231:NFORFP>2.0.CO;2

Gultepe, I., Fernando, H. J. S., Pardyjak, E. R., Hoch, S. W., Silver, Z., Creegan, E., et al. (2016). An overview of the MATERHORN fog project: Observations and predictability. *Pure and Applied Geophysics*, *173*(9), 2983–3010. https://doi.org/10.1007/s00024-016-1374-0

Gultepe, I., Pearson, G., Milbrandt, J. A., Hansen, B., Platnick, S., Taylor, P., et al. (2009). The fog remote sensing and modeling field project. *Bulletin of the American Meteorological Society*, *90*(3), 341–360. https://doi.org/10.1175/2008BAMS2354.1

Gultepe, I., Tardif, R., Michaelides, S. C., Cermak, J., Bott, A., Bendix, J., et al. (2007). Fog research: A review of past achievements and future perspectives. *Pure and Applied Geophysics*, *164*(6), 1121–1159. https://doi.org/10.1007/s00024-007-0211-x

Gultepe, I., Zhou, B., Milbrandt, J., Bott, A., Li, Y., Heymsfield, A. J., et al. (2015). A review on ice fog measurements and modeling. *Atmospheric Research*, *151*, 2–19. https://doi.org/10.1016/j.atmosres.2014.04.014

Hang, C., Nadeau, D. F., Gultepe, I., Hoch, S. W., Román-Cascón, C., Pryor, K., et al. (2016). A case study of the mechanisms modulating the evolution of valley fog. *Pure and Applied Geophysics*, *173*(9), 3011–3030. https://doi.org/10.1007/s00024-016-1370-4

Hong, S. Y. (2010). A new stable boundary-layer mixing scheme and its impact on the simulated East Asian summer monsoon. *Quarterly Journal of the Royal Meteorological Society*, *136*(651), 1481–1496. https://doi.org/10.1002/qj.665

Hong, S. Y., Noh, Y., & Dudhia, J. (2006). A new vertical diffusion package with an explicit treatment of entrainment processes. *Monthly Weather Review*, *134*(9), 2318–2341. https://doi.org/10.1175/MWR3199.1

Kain, J. S. (2004). The Kain–Fritsch convective parameterization: An update. *Journal of Applied Meteorology*, *43*(1), 170–181. https://doi.org/10.1175/1520-0450(2004)043<0170:TKCPAU>2.0.CO;2

Li, X., Gao, C. Y., Gao, Z., & Zhang, X. (2020). Atmospheric boundary layer turbulence structure for severe foggy haze episodes in north China in December 2016. *Environmental Pollution*, *264*, 114726. https://doi.org/10.1016/j.envpol.2020.114726

Li, X., Pu, Z., & Gao, Z. (2021). Effects of roll vortices on the evolution of Hurricane Harvey during landfall. *Journal of the Atmospheric Sciences*, *78*, 1847–1867. https://doi.org/10.1175/JAS-D-20-0270.1

Lin, C., Zhang, Z., Pu, Z., & Wang, F. (2017). Numerical simulations of an advection fog event over Shanghai Pudong International Airport with the WRF model. *Journal of Meteorological Research*, *31*(5), 874–889. https://doi.org/10.1007/s13351-017-6187-2

Maronga, B., & Bosveld, F. C. (2017). Key parameters for the life cycle of nocturnal radiation fog: A comprehensive large-eddy simulation study. *Quarterly Journal of the Royal Meteorological Society*, *143*(707), 2463–2480. https://doi.org/10.1002/qj.3100

Mazoyer, M., Lac, C., Thouron, O., Bergot, T., Masson, V., & Musson-Genon, L. (2017). Large eddy simulation of radiation fog: Impact of dynamics on the fog life cycle. *Atmospheric Chemistry and Physics*, *17*(21), 13017–13035. https://doi.org/10.5194/acp-17-13017-2017

Mlawer, E. J., Taubman, S. J., Brown, P. D., Iacono, M. J., & Clough, S. A. (1997). Radiative transfer for inhomogeneous atmospheres: RRTM, a validated correlated-k model for the longwave. *Journal of Geophysical Research*, *102*(D14), 16663–16682. https://doi.org/10.1029/97JD00237

Müller, M. D., Masbou, M., & Bott, A. (2010). Three-dimensional fog forecasting in complex terrain. *Quarterly Journal of the Royal Meteorological Society*, *136*(653), 2189–2202. https://doi.org/10.1002/qj.705

Nakanishi, M. (2000). Large-eddy simulation of radiation fog. *Boundary-Layer Meteorology*, *94*(3), 461–493. https://doi.org/10.1023/A:1002490423389

Pithani, P., Ghude, S. D., Chennu, V. N., Kulkarni, R. G., Steeneveld, G. J., Sharma, A., et al. (2019). WRF model prediction of a dense fog event occurred during the winter fog experiment (WIFEX). *Pure and Applied Geophysics*, *176*(4), 1827–1846. https://doi.org/10.1007/s00024-018-2053-0

Porson, A., Price, J., Lock, A., & Clark, P. (2011). Radiation fog. Part II: Large-eddy simulations in very stable conditions. *Boundary-Layer Meteorology*, *139*(2), 193–224. https://doi.org/10.1007/s10546-010-9579-8

Price, J. (2011). Radiation fog. Part I: Observations of stability and drop size distributions. *Boundary-Layer Meteorology*, *139*(2), 167–191. https://doi.org/10.1007/s10546-010-9580-2

Pu, Z. (2017). In S. K. Park, & L. Xu (Eds.), *Surface data assimilation and near-surface weather prediction over complex terrain. Data Assimilation for Atmospheric, Oceanic and Hydrologic Applications* (Vol. III, pp. 219–240). Springer. https://doi.org/10.1007/978-3-319-43415-5_10

Pu, Z., Chachere, C. N., Hoch, S. W., Pardyjak, E., & Gultepe, I. (2016). Numerical prediction of cold season fog events over complex terrain: The performance of the WRF model during MATERHORN-fog and early evaluation. *Pure and Applied Geophysics*, *173*(9), 3165–3186. https://doi.org/10.1007/s00024-016-1375-z

Román-Cascón, C., Steeneveld, G. J., Yagüe, C., Sastre, M., Arrillaga, J. A., & Maqueda, G. (2016). Forecasting radiation fog at climatologically contrasting sites: Evaluation of statistical methods and WRF. *Quarterly Journal of the Royal Meteorological Society*, *142*(695), 1048–1063. https://doi.org/10.1002/qj.2708

Román-Cascón, C., Yagüe, C., Sastre, M., Maqueda, G., Salamanca, F., & Viana, S. (2012). Observations and WRF simulations of fog events at the Spanish Northern Plateau. *Advances in Science and Research*, *8*(1), 11–18. https://doi.org/10.5194/asr-8-11-2012

Román-Cascón, C., Yagüe, C., Steeneveld, G. J., Morales, G., Arrillaga, J. A., Sastre, M., & Maqueda, G. (2019). Radiation and cloud-base lowering fog events: Observational analysis and evaluation of WRF and HARMONIE. *Atmospheric Research*, *229*, 190–207. https://doi.org/10.1016/j.atmosres.2019.06.018

Skamarock, W. C., Klemp, J. B., Dudhia, J., Gill, D. O., Liu, Z., Berner, J., et al. (2019). *A description of the advanced Research WRF ModelVersion 4* (pp. 145). NCAR Tech. Note NCAR/TN-5561STR.

Steeneveld, G. J., Ronda, R. J., & Holtslag, A. A. M. (2015). The challenge of forecasting the onset and development of radiation fog using mesoscale atmospheric models. *Boundary-Layer Meteorology*, *154*(2), 265–289. https://doi.org/10.1007/s10546-014-9973-8

Thompson, G., Rasmussen, R. M., & Manning, K. (2004). Explicit forecasts of winter precipitation using an improved bulk microphysics scheme. Part I: Description and sensitivity analysis. *Monthly Weather Review*, *132*(2), 519–542. https://doi.org/10.1175/1520-0493(2004)132<0519:EFOWPU>2.0.CO;2

Tudor, M. (2010). Impact of horizontal diffusion, radiation and cloudiness parameterization schemes on fog forecasting in valleys. *Meteorology and Atmospheric Physics*, *108*(1), 57–70. https://doi.org/10.1007/s00703-010-0084-x

Uematsu, A., Yamamoto, M. K., Hashiguchi, H., Hirashima, K., & Fukao, S. (2005). Shear-induced roll structure of fog observed by a millimeter-wave scanning Doppler radar. *Geophysical Research Letters*, *32*(14), L14824. https://doi.org/10.1029/2005GL022423

Van der Velde, I. R., Steeneveld, G. J., Schreur, B. W., & Holtslag, A. A. M. (2010). Modeling and forecasting the onset and duration of severe radiation fog under frost conditions. *Monthly Weather Review*, *138*(11), 4237–4253. https://doi.org/10.1175/2010MWR3427.1

Welch, R. M., & Wielicki, B. A. (1986). The stratocumulus nature of fog. *Journal of Applied Meteorology and Climatology*, *25*(2), 101–111. https://doi.org/10.1175/1520-0450(1986)025<0101:TSNOF>2.0.CO;2

Zhang, F., & Pu, Z. (2019). Sensitivity of numerical simulations of near-surface atmospheric conditions to snow depth and surface albedo during an ice fog event over Heber Valley. *Journal of Applied Meteorology and Climatology*, *58*(4), 797–811. https://doi.org/10.1175/JAMC-D-18-0064.1

Zhou, B., Du, J., Gultepe, I., & Dimego, G. (2012). Forecast of low visibility and fog from NCEP: Current status and efforts. *Pure and Applied Geophysics*, *169*(5), 895–909. https://doi.org/10.1007/s00024-011-0327-x